

Article

Design of In-Orbit Sample Container Transfer Mechanism for Chang'E-5 Lunar Sample Return Mission

Weijun Wang^{1,2}, Yuxin Cui³, Chenkun Qi^{1,*}, Yanyan Cao², Yuhua Zhang³, Chongfeng Zhang^{3,4} and Shigang Wang¹

¹ School of Mechanical Engineering, Shanghai Jiao Tong University, Shanghai 200240, China; basicnobel@163.com (W.W.); wangshigang@sjtu.edu.cn (S.W.)

² Shanghai Institute of Aerospace System Engineering, Shanghai 201109, China; caoyanyan236@126.com

³ Shanghai Academy of Spaceflight Technology, Shanghai 201109, China; fredcuimail@aliyun.com (Y.C.); 13501916238@139.com (Y.Z.); zhcf008@139.com (C.Z.)

⁴ Space Structure and Mechanism Technology Laboratory of China Aerospace Science and Technology Group Co., Ltd., Shanghai 201109, China

* Correspondence: chenkqi@sjtu.edu.cn

Abstract: In this paper, a pawl composite linkage transfer mechanism is designed for the automatic in-orbit sample transfer mission of Chang'E-5 lunar sample return mission, which can realize the sample container in-orbit transfer under various critical constraints such as lightweight, miniaturization, and narrow working space. Resistance during the whole process as well as the sensitive factors that affect the resistance during the sample container transfer process are investigated and designed. The sample container transfer process has been verified by the test system on the ground, indicating that the design can satisfy the requirements of the sample transfer mission. The developed transfer mechanism completed the Chang'E-5 sample return mission successfully with good consistency between space and ground, verifying the correctness and effectiveness of the design.

Keywords: mechanism design; transfer mechanism; in-orbit transfer; sample return mission; Chang'E-5



Citation: Wang, W.; Cui, Y.; Qi, C.; Cao, Y.; Zhang, Y.; Zhang, C.; Wang, S. Design of In-Orbit Sample Container Transfer Mechanism for Chang'E-5 Lunar Sample Return Mission. *Aerospace* **2023**, *10*, 992. <https://doi.org/10.3390/aerospace10120992>

Academic Editor: Hyun-Ung Oh

Received: 24 October 2023

Revised: 20 November 2023

Accepted: 23 November 2023

Published: 25 November 2023



Copyright: © 2023 by the authors. Licensee MDPI, Basel, Switzerland. This article is an open access article distributed under the terms and conditions of the Creative Commons Attribution (CC BY) license (<https://creativecommons.org/licenses/by/4.0/>).

1. Introduction

China's lunar exploration project consists of three steps: circling, landing, and returning. Chang'E-5's mission is to collect lunar soil from previously unexplored areas of the moon and return it to Earth. The mission is one of the most complex in China's lunar exploration project [1–3]. The mission is the first lunar sampling return mission after more than 40 years of sampling missions by the United States and the former Soviet Union. Scientists can use these new samples to learn more about the formation of the moon and a more comprehensive picture of its geology. In order to realize the return mission of lunar samples to the Earth, the United States completed six manned lunar landings through the Apollo Program from November 1969 to December 1972 and finally brought back about 385 kg of lunar samples. The former Soviet Union completed three unmanned sample return missions through the Lunar Series Probe from September 1970 to August 1976, which adopted a direct lunar surface takeoff and return to Earth, and brought back 101 g, 55 g, and 170 g of lunar soil, respectively [4–6]. Unlike the United States and the former Soviet Union, China adopted the Unmanned Probe Program of automatic rendezvous and docking in lunar orbit, which is more cost-effective and technologically advanced than the United States and the former Soviet Union and lays the technical foundation for subsequent manned lunar exploration missions [7–9]. Chang'E-5 consists of a lunar orbiter, a re-entry vehicle, a lunar lander, and a lunar ascender. After the spacecraft enters lunar orbit, the combination of lander and ascender will separate and descend to the Rumke Mountains region of the lunar surface. After the lunar surface completes the sampling, the lunar ascender will take off from the lunar surface and dock with the components of

the lunar orbiter and re-entry vehicle, as shown in Figure 1. After completing the in-orbit rendezvous and docking, Chang'E-5 will complete the automatic in-orbit transfer of the sample container between the lunar ascender and the re-entry vehicle.

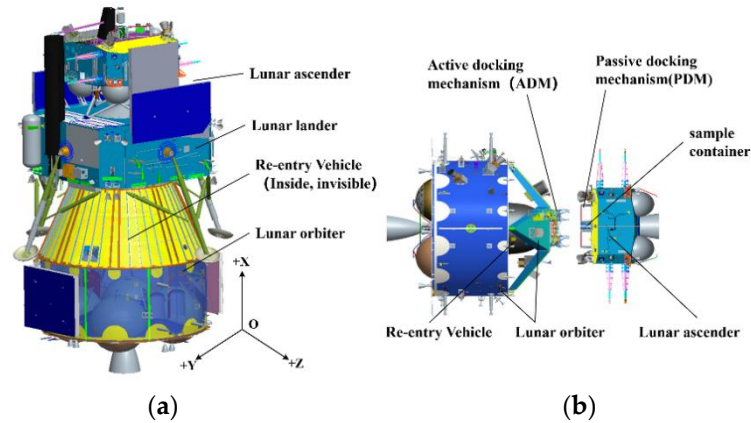


Figure 1. Launch and docking configuration of Chang'E-5 probe. (a) Launch configuration. (b) Docking configuration.

The sample container (SC), which enables reliable encapsulation of samples [8,10], has a base size of $\text{Ø}180 \text{ mm} \times 260 \text{ mm}$ with localized protrusions, and a total mass of about 7 kg, including about 2 kg of lunar samples; see Figure 2.

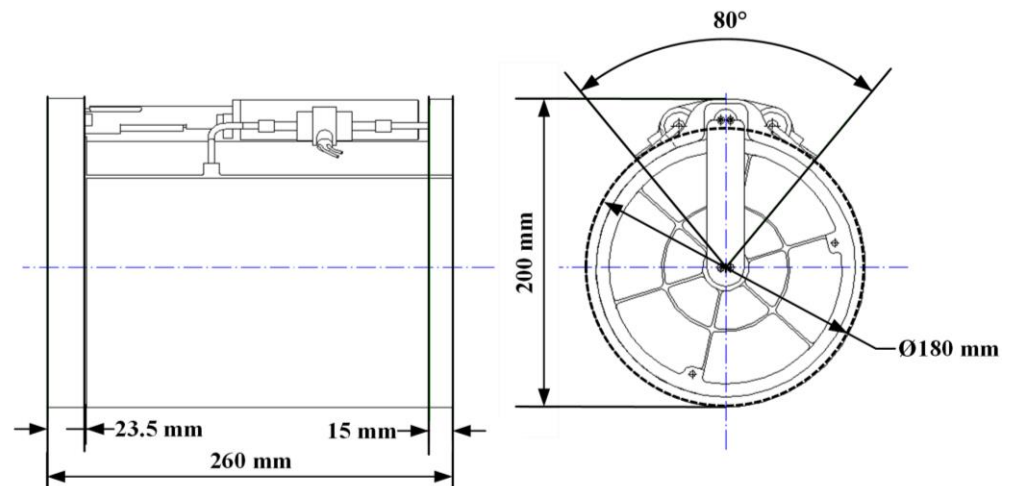


Figure 2. External dimensions of sample container.

The layout of the spacecraft has been optimized with a peripheral docking mechanism [11,12], in which all the equipment is arranged in a ring area around the center, and the center position is left as a channel for the transfer of SC. The transfer path of the sample container has been simplified to a straight line, but the automated in-orbit transfer of sample containers between the lunar ascender, the lunar orbiter, and the re-entry vehicle is still required. The initial position of the sample container is in the lunar ascender, and the target position is in the re-entry vehicle, with an intermediate pass through the lunar orbiter. The total transfer distance is no less than 626 mm. In order to overcome the various friction and guiding resistance forces, the transfer push force should be no less than 50 N. The whole transfer process requires precise coordination of the different parts [13] and simultaneously a consideration of multiple constraints on mass, envelope, and autonomous control. Generally, after the completion of space docking, a multi-degree-of-freedom robot arm is utilized in order to realize the transfer of objects between manned or unmanned

crafts in near-Earth orbit, such as China Space Station, International Space Station, space shuttle, the Orbital Express, the ETS-VII, etc. [14–18]. The multi-degree-of-freedom space robot arm has the advantages of a large moving range, flexibility of movement, high repeatability, etc. However, its motion control requires ground remote control support, and the mass, size, and motion envelope are too large to be applicable in deep space exploration missions. Complex linkage mechanisms are often used in the design of space mechanisms to realize the spreading and retracting functions, but they cannot satisfy the functions of grasping and releasing objects [19]. In the Chang'E-5 probe mission, the sample transfer mechanism is required to meet the needs of large stroke, lightweight, miniaturization, etc., and the existing transfer mechanisms cannot satisfy these requirements.

The automated sample container in-orbit transfer mission is to transfer the sample container automatically from the lunar ascender to the re-entry vehicle during the flight of the assembly to ensure that the sample containers are able to proceed to the subsequent mission. The lightweight design of the entire lunar sample return probe is very strict; thus, the transfer mechanism is designed according to the principles of lightweight and system optimization. Theoretically, the transfer mechanism can be mounted on any of the ascender, the orbiter, or the re-entry vehicle to fulfill the functional requirements. However, the mounting location makes a significant difference in terms of the launch mass cost of the system. The lunar ascender and the re-entry vehicle are more mass-sensitive, so mounting the transfer mechanism either on the ascender or on the re-entry vehicle could result in a greater mass cost for the launch. Therefore, the transfer mechanism is prioritized for mounting on the lunar orbiter, which could reduce the design difficulty of the ascender and the re-entry vehicle so that the principle of lightweight design is better followed. In this kind of layout, the transfer mechanism needs to accomplish three tasks:

- (a) Initial capture of the container: At the beginning, the transfer mechanism and the sample container are on two different crafts, the lunar orbiter and the lunar ascender. Before the start of the transfer, the transfer mechanism should be able to overcome a certain initial deviation and realize a reliable capture of the sample container.
- (b) Automatic and smooth transfer of the sample container: The controlled movement of the sample container is about 626 mm from the initial position in the lunar ascender to the target position in the re-entry vehicle. The transfer process should be adapted to possible positional deviations and frictional resistance and should maintain a smooth movement of the sample container to avoid additional impact loads that may cause structural damage to the container.
- (c) Automatic recovery: After the completion of the sample container transfer, the transfer mechanism should be capable of being reset and retracted in order to facilitate the hatch close of the re-entry vehicle.

To accomplish these tasks, this paper innovatively proposes a pawl composite linkage sample transfer mechanism and also studies the difficulties during the transfer process such as the design of the resistance, etc. The second part of this paper describes the general design and working process of the transfer mechanism. The third part introduces the resistance analysis of the transfer process. The fourth part describes the analysis and the validation of the in-orbit mission. The design of the mechanism is mainly based on an exploratory research method. Preliminary verification has been carried out through quantitative analysis and simulation methods. On the basis of the theoretical analysis of the mechanism design, a transfer process model was established using MATLAB R2014a for simulation analysis, and a transfer test system on the ground was set up to verify its performance. The design was examined through the flight mission. The last part is the conclusion.

2. General Design of the Transfer Mechanism

2.1. Composition and Configuration

A pawl composite linkage sample transfer mechanism is proposed through comprehensive design to accomplish the sample transfer mission and fulfill the functional requirements of the sample transfer.

In order to solve the functions of motion trajectory constraint, transfer motion control, and container grasping and releasing during the transfer process, respectively, the transfer mechanism consists of three parts: guide rails, push-puller, and the attachment on the SC. Accurate coordination and balance between the three parts are needed to ensure the feasibility of the scheme design; see Figure 3.

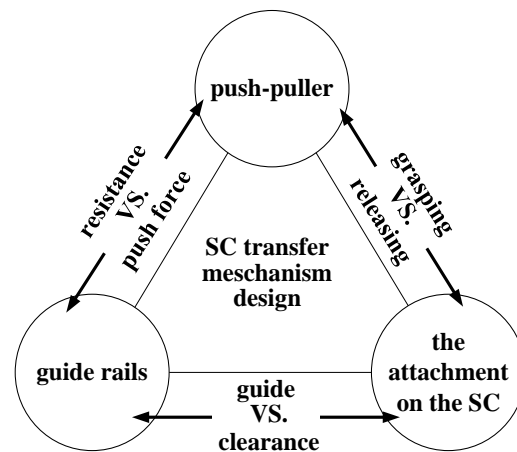


Figure 3. Coordination and balance between the three parts.

The first part is the guide rail, which forms a transfer channel to provide support and guidance for the transfer process. It could also adapt to the positional deviation between different crafts to ensure that the transfer movement is free of stagnation. The second part is the push-puller, which is used to realize the active movement of the sample container. The push-puller could provide stable and controllable force to overcome the resistance during the transfer process. The third part is the attachment on the sample container, which is the guide cylinder and the ratchet structure on the sample container for use in conjunction with the guiding and transfer process; see Figure 4.

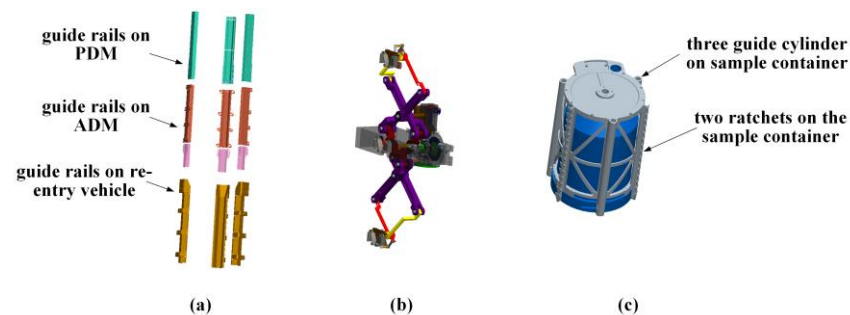


Figure 4. Composition of the sample transfer mechanism. (a) guide rails. (b) push-puller. (c) the attachment on the sample container.

The sample transfer mechanism is designed based on the peripheral docking mechanism. Together with the claw-type docking mechanism, it forms the Chang'E-5 docking mechanism and sample transfer mechanism. To increase the reliability of the task, two sets of completely independent push-pullers are arranged symmetrically at 120 degrees in the circumferential direction of the transfer channel. The two sets of mechanisms can work independently or jointly as a backup for each other [20]. The motors of both sets of

mechanisms are double-winding motors to ensure reliability. The layout and configuration of the sample transfer mechanism are shown in Figure 5.

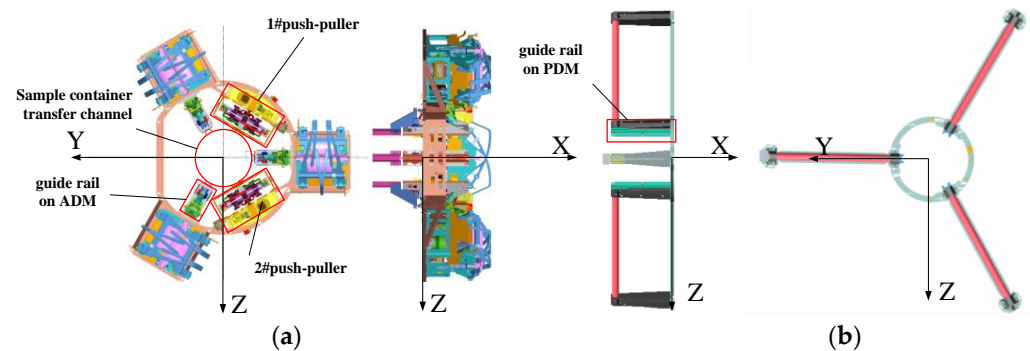


Figure 5. The docking mechanism and transfer mechanism layout. (a) Active docking mechanism (ADM). (b) Passive docking mechanism (PDM).

2.2. Detailed Design of Transfer Mechanism

2.2.1. Guide Rails

The guide rails form the transfer path of the sample container and provide guidance and support. The guide rails consist of three segments distributed in the ascender, the orbiter, and the re-entry vehicle. During the transfer process, the sample container would pass through the passive part of the docking and sample transfer mechanism (PDM), active part of the docking and sample transfer mechanism (ADM), and the re-entry vehicle from the initial position, and finally arrive at the target position. In order to ensure that the transfer function is carried out successfully, structures with guiding functions are arranged at each of the above segments, which could be coordinated with the corresponding guiding structures on the sample container (see Section 2.2.3) to ensure that the moving process of the sample container could be straight. Through the optimization of the design and analysis of the guiding structure, the design of the guiding structure is shown in Figure 6. According to the layout configuration, the guide rails are divided into three sections, guide rails on PDM, guide rails on ADM, and guide rails on the re-entry vehicle, with lengths of 217 mm, 265 mm, and 270 mm, respectively. The three parts of the guide rails are mounted on different crafts, and the intervals between them are 19 mm and 40 mm, respectively. The total stroke of the transfer is 626 mm. Considering the positioning error between the active and passive docking mechanism, the manufacturing and installation deviation of the large-size vehicle structure, and the influence of environmental high or low temperature, the coaxiality deviation between the three sections of the guide rails is more than ± 0.5 mm and ± 5 mm. In order to ensure that the sample container can smoothly enter the next section, it is required that the next section of the guide rail can accommodate the coaxiality deviation between the previous section of the guiding gap and the guide rail. Therefore, the guiding gap is designed to be enlarged gradually. In addition, at the transition between the two sections of the guide rails, a guiding cone is provided at the front end of the guide rail of the next section.

In order to ensure that the five degrees of freedom of the container, except for the axial movement direction, are effectively restrained, the guide rail is designed as a trapezoidal cross-section, and the guide cylinder is a semi-circular structure mounted on the outside of the sample container. The cross-sectional layout of the guide structure and the guide cylinder are shown in Figure 7.

To adapt to the deformation caused by high or low temperatures and other deviations, the minimum gap between the guide rail and the guide cylinder is 1 mm. According to the need for tolerance, each section of the guide rail set up a gradually enlarged gap. The size of each section of the guide rail and the gap is designed in Table 1.

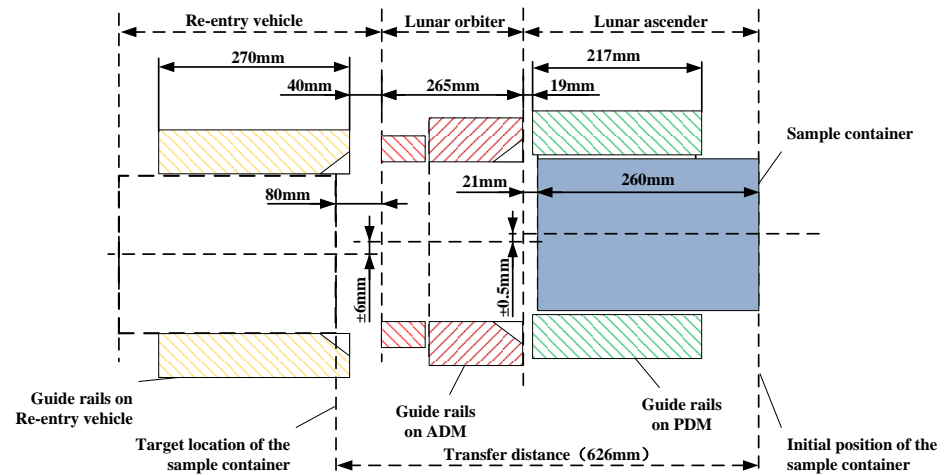


Figure 6. Schematic representation of the guide rail.

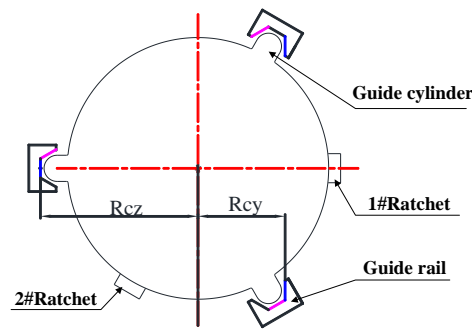


Figure 7. Layout of the guide structure section.

Table 1. Size design of the guide rail.

No.	Item	Sample Container	Guide Rails on PDM	Guide Rails on ADM		Guide Rails on Re-Entry Vehicle
				Fixed Part	Retractable Part	
1	Length (mm)	260.0	217.0	185.0	75.0	270.0
2	Distance from center (mm)	106.0	107.0	107.8	108.5	110.5
3	Nominal gap to container (mm)	/	1.0	1.8	2.5	4.5
4	Angle of distribution (°)			120		

In order to meet the demand of avoiding space after completing the transfer, the guide rail on ADM is designed as a partially retractable configuration, the length of the retracted part is 75 mm, and it could automatically retract through the pyrotechnically actuated separation devices and the torsional spring; see Figure 8.

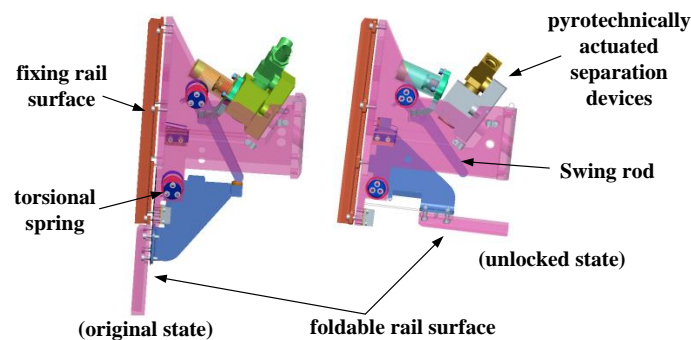


Figure 8. Retraction function of the guide rail on ADM.

2.2.2. Push-Puller

The push-puller mechanism is based on the principle of a retractable planar composite linkage mechanism, which realizes a wide range of movement in the narrow channel and automatic grabbing of containers, etc. Two ratchet-pawl mechanisms are mounted at the ends of the push-puller, and a drive unit is mounted in the middle. The output of the drive unit is linear movement, which could drive the intermediate pin of the composite linkage mechanism to move. Through a parallel combination of the parallel linkage mechanism, the amplification of the stroke of the drive mechanism is realized. Under the constraints of the layout and the transfer stroke, the design of the push-puller has a height of 581 mm in the deployed state, and 177 mm in the folded state. To realize the precise control of the push-puller, a rotary transformer is installed to monitor the position change of the mechanism. The schematic diagram of the push-puller is shown in Figure 9a. The dotted line in the figure shows the deployed state of the compound linkage, and the solid line shows the folded state of the compound linkage. Figure 9b shows the deployed state of the push-puller, and Figure 9c shows the folded state. The push-puller could be repeatedly extended a number of times according to the control instructions to realize an accumulation of the transfer distance.

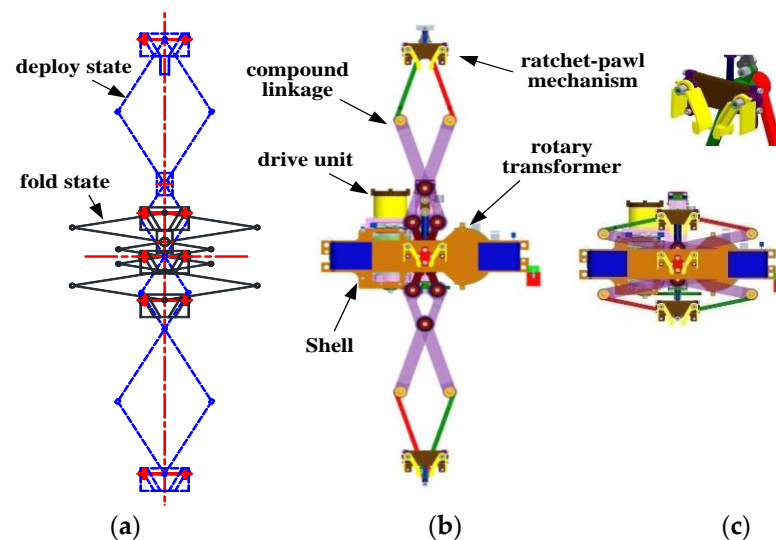


Figure 9. Working principle and detailed design of push-puller. (a) Schematic diagram. (b) Deployed state of push-puller. (c) Folded state of the push-puller.

In order to realize the functions of capturing, maintaining the connection state, and automatic release between the transfer mechanism and the sample container, a pawl mechanism is designed and mounted at the end of the linkage. There are four sets of pawls, three of which are mounted on the push-puller mechanism and one on the re-entry vehicle. The ratchet that corresponds to the pawls is mounted on the outside of the sample container (see Section 2.2.3 for details). The working principle of the pawl and ratchet is shown in Figure 10. To realize the functions of capture, unidirectional movement, and release of the pawl to the ratchet, five states occur in sequence between the pawl and the ratchet:

- (a) Firstly the ratchet is kept still and the pawl is driven by the push-puller close to the ratchet (Figure 10a).
- (b) The pawl continues to move forward and contact with the ratchet, both of which are designed with a tolerant rake angle to accommodate the initial capture (Figure 10b).
- (c) The pawl continues to move forward. Under the influence of the push force, the pawl overcomes the torsional spring and passes through the ratchet on the rack in turn (Figure 10c).
- (d) After the pawl moves to the maximum position, it starts to move backward driven by the push-puller. Due to the unidirectional movement characteristics of the pawl and

- the ratchet, the ratchet and the pawl remain relatively stationary, driving the sample container backward until the push-puller is withdrawn in place (Figure 10d).
- (e) When the push-puller deploys again, the ratchet engages with other pawls and remains still, and the original pawl could be naturally disengaged from the ratchet of the sample container under the driving force of the push-puller so that the sample container is finally released (Figure 10e).

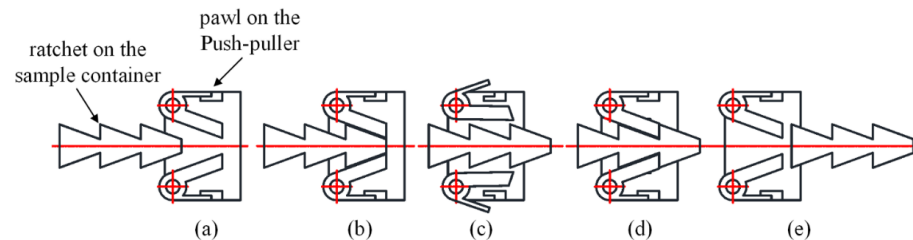


Figure 10. Working principle of the pawl mechanism. (a) Initial state. (b) Contact. (c) Pass through. (d) Drive backward. (e) Release.

2.2.3. Attachment on the Sample Container

The detailed design of the guide rails and the push-puller specified the attachments on the outside of the sample container, including three guide cylinders and two ratchets. Figure 11a is the design model while Figure 11b is the actual product.

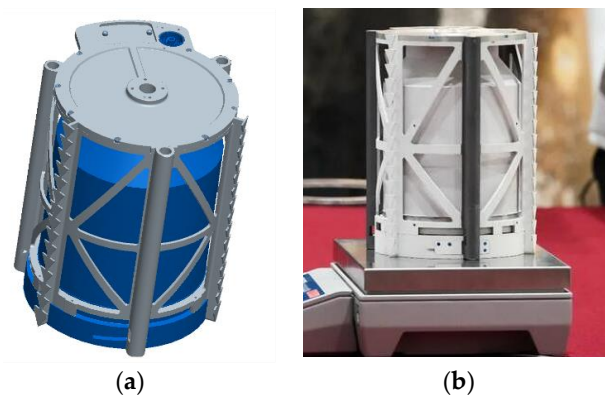


Figure 11. Diagram of sample container. (a) Design model. (b) Actual product.

2.3. Working Process

The whole transfer process is completed by the push-puller with four cycles of stretching. During the transfer, multiple sets of pawls cooperate with each other to move the sample container. The push-puller moves the pawls over a wide range by deploying and folding repeatedly, and the sample container moves unidirectionally under the impact of pawls in conjunction with ratchets. The removable pawls at both ends allow multiple pull-back and push-out functions while the pawls in the middle position and in the re-entry vehicle are fixed to the structure to maintain the position of the sample container during transfer. Transfer of the sample container to the target position in the re-entry vehicle is realized through deploying and folding repeatedly. The detailed process can be divided into nine steps below, also shown in Figure 12:

- (a) Initial state of the sample container before transfer.
- (b) The push-puller deploys for the first time, and the #1 pawl captures the sample container.
- (c) The push-puller folds for the first time, the sample container moves forward about 190 mm driven by the #1 pawl, and the #2 pawl captures the container.
- (d) The push-puller deploys for the second time, the sample container remains still under the capture of the #2 pawl, and the #1 pawl releases the container.

- (e) The push-puller folds for the second time, the sample container moves forward to about 327 mm under the action of the #2 pawl, and the #3 pawl captures the container.
- (f) The push-puller deploys for the third time, and the sample container moves forward to 508 mm under the action of the 3#3 and enters the re-entry vehicle, while the lock (#4 pawl) in the re-entry vehicle captures the container.
- (g) The push-puller folds for the third time, the sample container remains still under the capture of the #4 pawl, and the #3 pawl releases the container.
- (h) The push-puller deploys for the fourth time, the sample container moves forward under the action of #4 pawl, and the container moves to the target position in the re-entry vehicle.
- (i) The push-puller folds for the fourth time and resets to the initial position, and the guide rails on ADM are retracted.

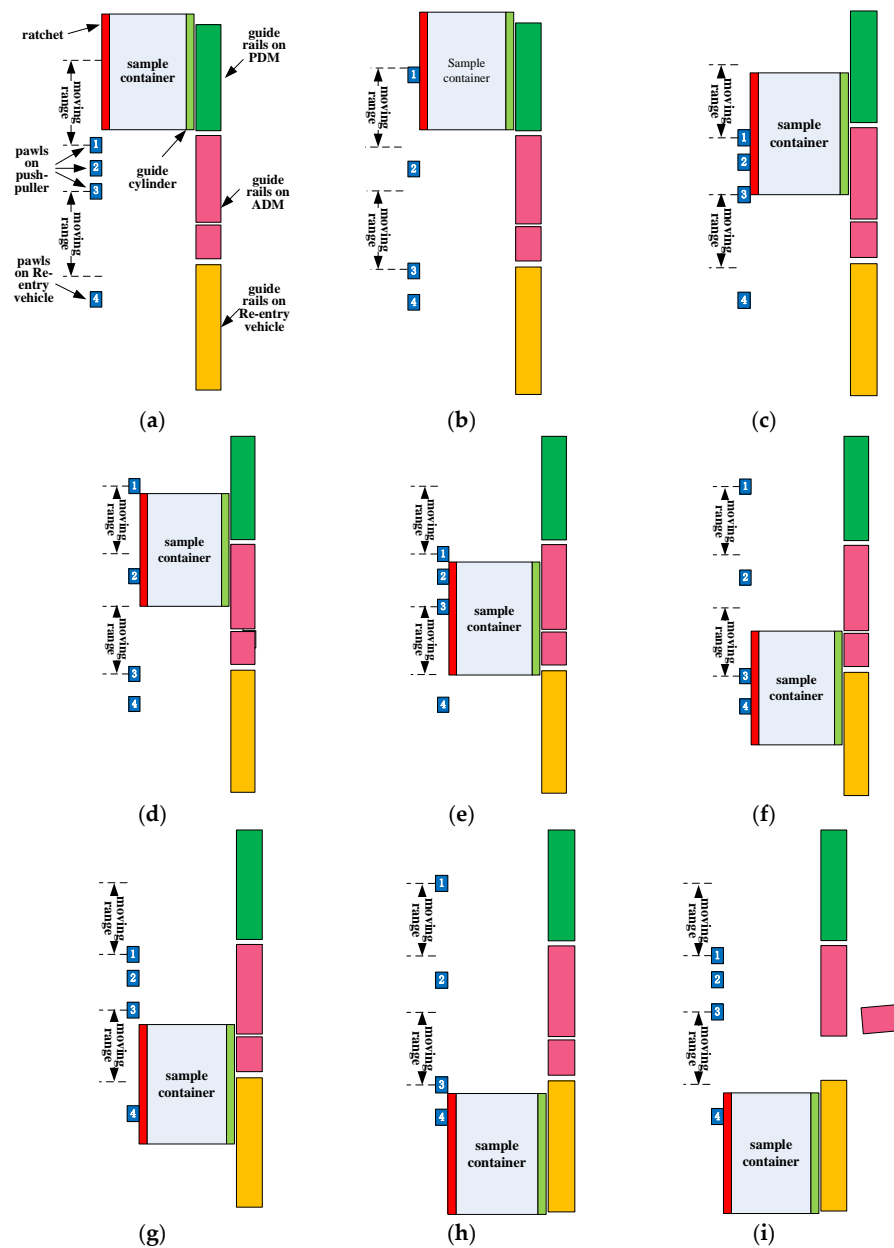


Figure 12. Working process of the transfer mechanism. (a) Initial state. (b) The first deployment. (c) The first retract. (d) The second deployment. (e) The second retract. (f) The third deployment. (g) The third retract. (h) The fourth deployment. (i) The fourth retract (include guide rails).

Using MATLAB to calculate and analyze the transfer process, the result of the transfer stroke over time is shown in Figure 13. The simulation shows that the maximum transfer stroke reaches 641 mm, which meets the requirement of no less than 626 mm.

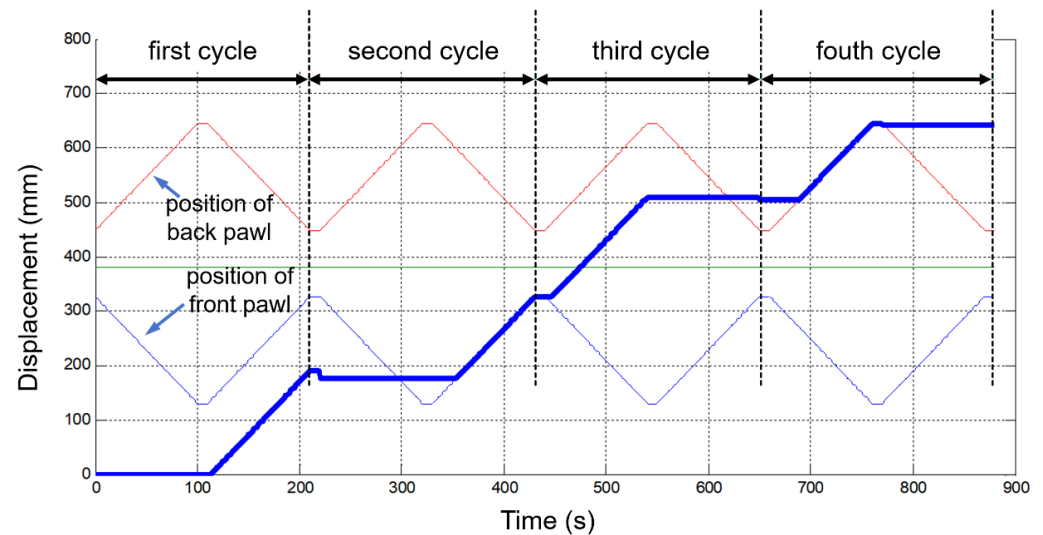


Figure 13. The simulated result of transfer stroke over time.

3. Resistance Analysis of the Transfer Process

The control and overcoming of the resistance forces, such as friction, lock-in-place triggering force, and faulty pawl passage during the transfer process is one of the difficulties for a successful completion of the transfer. In normal conditions, there are two sets of transfer mechanisms that work simultaneously to transfer the sample container. However, when one set of transfer mechanisms breaks down, another set of transfer mechanisms should still complete the transfer task. In this condition, the external resistance of the transfer process increases slightly, which is a typical working condition for transfer resistance analysis.

The resistance load during the transfer process mainly comes from three aspects:

- The frictional resistance generated by the contact between the guide rails and the guiding surface of the sample container. It is related to the overturning moment on the container, the effective length of the guide rail, and the coefficient of friction of the guiding surface.
- The resistance load of the container in contact with the one-way lock or locking mechanism of the sample compartment of the re-entry vehicle. The trigger force of a single set of locking mechanisms is designed to be less than 5 N.
- The resistance load when the container passes through a non-operating pawl. The passing resistance of a single set of pawl mechanisms is designed to be less than 5 N.

During the transfer process, the sample container passes through the guide rails on PDM, ADM, and the guide rails on the re-entry vehicle in turn. Therefore, the force condition of the sample container during the transfer process could be categorized into the following two types:

- Force condition of the sample container in one single segment of the guide rail. In this state, the sample container moves in a single segment of guide rail, and it is deflected by the driving force F of the transfer mechanism. The guide rails on PDM, ADM, or re-entry vehicle act with the guiding structure on the sample container to generate friction, and the driving force F overcomes this friction force f and the resistance force F_z to push the sample container moving forward.
- Force condition of the sample container as it enters the transition segment of the next guide rail. When the sample container enters the transition segment of the next guide rail, the back end of the guiding structure interacts with the previous guide rail to

generate position pressure and friction, and the front end of the guiding structure interacts with the angled surface of the next guide rail to generate positive pressure and friction. The driving force F overcomes the friction force f and the resistance force F_z to push the sample container moving forward.

The external resistance and force condition changes as the transfer process changes. Therefore a detailed analysis of the sensitive factors affecting transfer resistance and the resistance during the whole process is needed.

3.1. Analysis of Resistance Sensitive Factors

Taking the movement of the sample container in the single-segment guide rail as an example, the points of action of the force between the sample container and the guide rail are A and B, as shown in Figure 14.

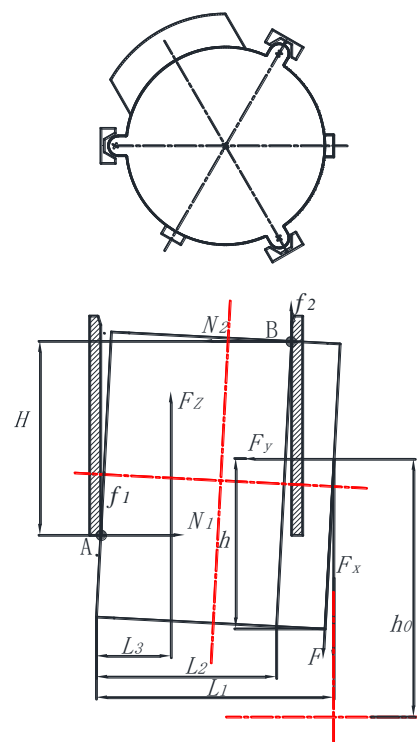


Figure 14. In-orbit force analysis of the substantive guide structures of the sample container.

The mechanical equations of the sample container could be obtained:

$$\begin{cases} N_1 + F_y = N_2 \\ F_z + f_2 + f_1 = F_x \\ F_x \times L_1 + F_y \times h_1 = f_2 \times L_2 + N_2 \times H + F_z \times L_3 \\ F_x = F \times \cos \beta \\ F_y = F \times \sin \beta \\ f_2 = N_2 \times \mu \\ f_1 = N_1 \times \mu \end{cases} \quad (1)$$

where F is the driving force provided by the transfer mechanism; N_1, N_2 are the support forces of the guide rail on the sample container; f_1, f_2 are the friction between the guide rail and the sample container; μ is the coefficient of friction; F_z is the resistance of the pawl of the fail-over mechanism to the sample container; F_x is the x-direction component of the drive force F , and F_y is the y-direction component of the drive force F ; L_1 is the force arm of axial force from the pawl of the transfer mechanism to the sample container with respect to the pivot point A; L_2 is the force arm of the friction force at pivot point B with respect to

pivot point I; L_3 is the force arm of the resistance F_z with respect to the pivot point A; H is the effective length of the guide rail; h_1 is the force arm of radial force from the pawl of the transfer mechanism to the sample container with respect to the pivot point A; β is the angle between the force acting on the sample container by the transfer mechanism and the axis.

Taking different friction coefficients, the ratio of F to F_z (power ratio) is plotted with respect to the effective length of guide rail H as shown in Figure 15. From the curves, it can be seen that in the single-segment guide structure, the required driving force F for the sample container increases rapidly with the decrease in the effective length of the guide rail and the increase in the friction coefficient. In the design, through the combination of multi-segment guide mechanism design, the whole effective length of the guide rail is guaranteed to be no less than 185 mm. Titanium alloy is used for the guiding structure, and MoS_2 is splashed on the surface of the guide cylinder of the sample container, which ensures that the coefficient of friction for relative motion is less than 0.2.

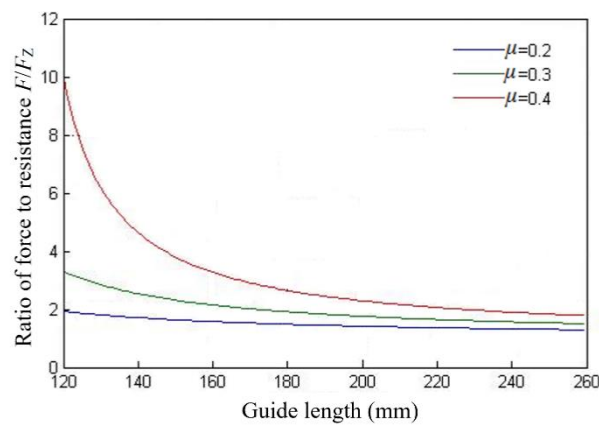


Figure 15. Variation curves of the power ratio with the guide stroke.

3.2. Calculation of Resistance for the Whole Process

The analysis above shows that the driving force of the transfer is more sensitive to the coefficient of friction. When the effective length of the guide rail is short, the drive force increases exponentially. Therefore, in order to ensure the reliability of the transfer process, analytical calculations of the drive force during the whole transfer process are carried out. The attitude deflection of the sample container under the push force of the transfer mechanism and force condition are shown in Figure 16. The equations are constructed according to the force balance as follows:

$$\begin{cases} F_{12} = f_1 + f_2 + F_3 + F_4 + F_5 + F_6 \\ F_1 = F_2 \\ f_1 = \mu F_1 \\ f_2 = \mu F_2 \\ M_O = F_3 L_1 + (f_2 + F_6) L_2 + (F_4 - F_{12}) L_3 + F_2 L_4 = 0 \end{cases} \quad (2)$$

$$F_{12} = f(\mu, L_1, L_2, L_3, L_4) \quad (3)$$

where F_{12} is the drive force provided by the transfer mechanism; F_1 and F_2 are the positive pressure provided by the left and right side of guiding structures; f_1 and f_2 are the friction force of the left and right side of guiding structures; μ is the coefficient of friction; F_3 is the resistance of the non-operating pawl; F_4 is the one-way lock resistance in the container compartment of re-entry vehicle; F_5 and F_6 are the resistance of locking mechanism in the re-entry vehicle; L_1 is the distance between the non-operating pawl and the left guide structure of the compartment; L_2 is the distance between the left guide structure and the right one; L_3 is the distance between the pawl in working state and the left guide structure;

L_4 is the guiding length during the transfer process; and M_O is the combined moment at point O.

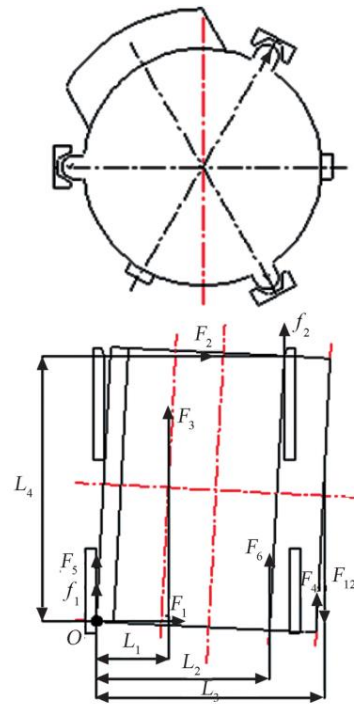


Figure 16. In-orbit force analysis of the transfer mechanism.

L_1 , L_2 , and L_3 are constants when the size and other parameters of the guiding structure configuration are determined. As a result, the drive force only relates to the coefficient of friction μ and L_4 . L_4 is the guiding length. When the sample container is in a single segment of the guide rail, it is the length of the current guide structure. When the sample container is in the transition segment of the guide rail, it is the length of the guide strip on the sample container. So L_4 is also a definite value that varies with the transfer process.

According to the variation of the transfer stroke, transfer resistance, size, and configuration of the guiding structure, by using MATLAB to establish the resistance analysis program of the whole transfer process, the evolution of the resistance with respect to transfer stroke is obtained in Figure 17. The analysis takes the example of a single set of transfer mechanisms. The resistance that the transfer mechanism has to overcome varies at different positions of the transfer stroke. The maximum resistance during the whole transfer process occurs at the final locking stage of the container, with a maximum resistance of about 44 N. At this point, the sample container needs to overcome the resistance of a total of two sets of unidirectional pawls and three sets of locking mechanisms in the re-entry vehicle. The thin blue line in Figure 16 shows the change in resistance after an abnormal unlocking of the guide mechanism, resulting in a reduction in the effective length of the guide rail. During the whole transfer process, there are four resistance peaks, where the maximum resistance reaches 50 N. Therefore, considering the necessary margin of the driving capacity and the structural strength of the transfer mechanism, the design value of the transfer force for a single set of transfer mechanisms is determined to be 100 N.

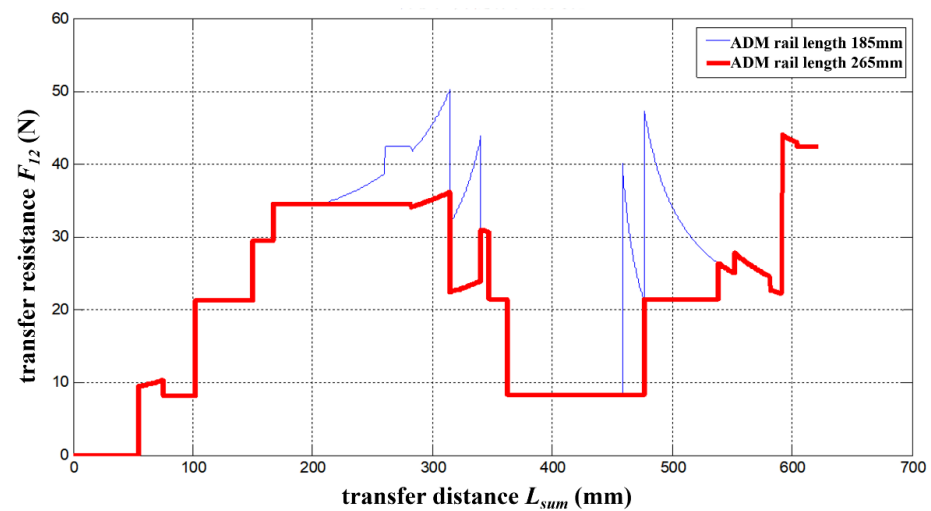


Figure 17. Result of force analysis during transfer process.

4. Validation

4.1. Experimental Validation

In order to verify the correctness of the sample transfer design, the whole process of sample container in-orbit transfer is assessed and verified. A transfer testing system on the ground was developed, as shown in Figure 18. The system consists of an upper platform and a lower platform, both of which are configured with a six-degrees-of-freedom relative motion capability to simulate a six-way positional deviation between the lunar ascender and the orbiter. The simulated compartment of the sample container is mounted on the lower platform. The initial position deviation between the re-entry vehicle and the lunar orbiter is simulated by setting the initial position deviation in the six degrees of freedom through the parallel Stewart mechanism. Sample containers and the re-entry vehicle in the test system are simulated by interface-equivalent simulation parts to realistically simulate the interface related to the transfer process such as ratchets, guide rails, positioning pins, etc. The gravity of the sample container mockup is counteracted by a follower-controlled hanging system, with the lifting point set at the center of mass of the mockup to simulate weightlessness in lunar orbit. In addition, the follower system could also be set to maintain a constant force to test the performance of the transfer force.

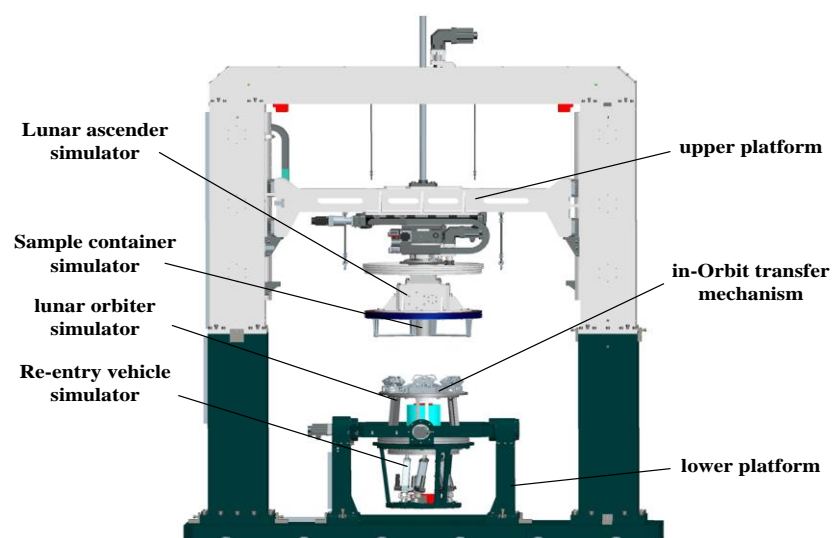


Figure 18. In-orbit transfer testing system.

The transfer tolerance validation test was carried out with a 5 mm deviation on the center axis between the orbiter and the re-entry vehicle, with one single set of transfer mechanisms and two sets of transfer mechanisms working. The working current of the transfer mechanism, the position of the sample container, the moving speed, and the working time could be monitored during the test. The conversion formula between the output of the push-puller and the motor current is shown in Equation (4):

$$F = \frac{I \cdot I_T \cdot \eta_1 \cdot \eta_2 \cdot i_{all}}{3} \approx 254I \quad (4)$$

where I is the working current of the motor. $I_T = 115$ mNm/A is the motor torque constant; $\eta_1 = 0.2$ is the transmission efficiency of the reducer; $\eta_2 = 0.75$ is the transmission efficiency of the parallel linkage; the transmission amplification of the parallel linkage mechanism is 3; and $i_{all} = 44$ mm⁻¹ is the equivalent reduction ratio of the screw-nut drive mechanism.

The test results show that the transfer process is successful, the transfer mechanism works smoothly, and the transfer current under different deviations does not differ much, which could better adapt to a variety of deviation working conditions. The test data are shown in Table 2. The maximum resistance during the transfer is no more than 40.64 N, which is in good agreement with the theoretical analysis results (44 N) and verifies the correctness of the analysis of the transfer design. The measured transfer resistance is slightly less than the theoretical value, indicating that the transfer mechanism has reached a better state in terms of sensitive control factors such as the coefficient of friction. In addition, a variety of transfer mechanism verification tests under tightened resistance and high or low-temperature environments were carried out to fully assess the transfer capability of the transfer mechanism.

Table 2. Data of transfer verification test.

No.	Test Conditions	Maximum Current (A)	Maximum Transfer Resistance (N)
1	Transfer mechanism 1#working	+Y 5 mm	27.94
2		−Y 5 mm	30.48
3		+Z 5 mm	30.48
4		−Z 5 mm	38.10
5	Transfer mechanism 2#working	+Y 5 mm	27.94
6		−Y 5 mm	25.40
7		+Z 5 mm	27.94
8		−Z 5 mm	40.64
9	Two transfer mechanism working	+Y 5 mm	38.10
10		−Y 5 mm	20.32
11		+Z 5 mm	25.40
12		−Z 5 mm	25.40

4.2. In-Orbit Flight Validation

At 6:10 p.m. on 6 December 2020, thirty minutes after the Chang'E-5 probe completed China's first lunar orbital rendezvous and docking mission, the Chang'E-5 probe successfully completed the first international in-orbit automatic transfer of sample container and completed the first retrieval of moon rocks in 40 years, as shown in Figure 19. This lays a solid foundation for the successful entry of the sample container into the target position of the re-entry vehicle and into the subsequent flight profiles. During in-orbit operation, the motor current, movement position, time and temperature, and other data of the two sets of sample transfer mechanisms were monitored. The effective working current range of the transfer mechanism is 0.08 A~0.18 A, and the temperature telemetry value is between −20.6 °C~+10.4 °C. The transfer mechanism completed the specified actions in sequence according to the designed state in 661 s (designed for 657 s). The consistency between space and ground is great. The successful completion of the in-orbit mission

demonstrated the correctness and effectiveness of the overall design of the pawl composite linkage transfer mechanism.

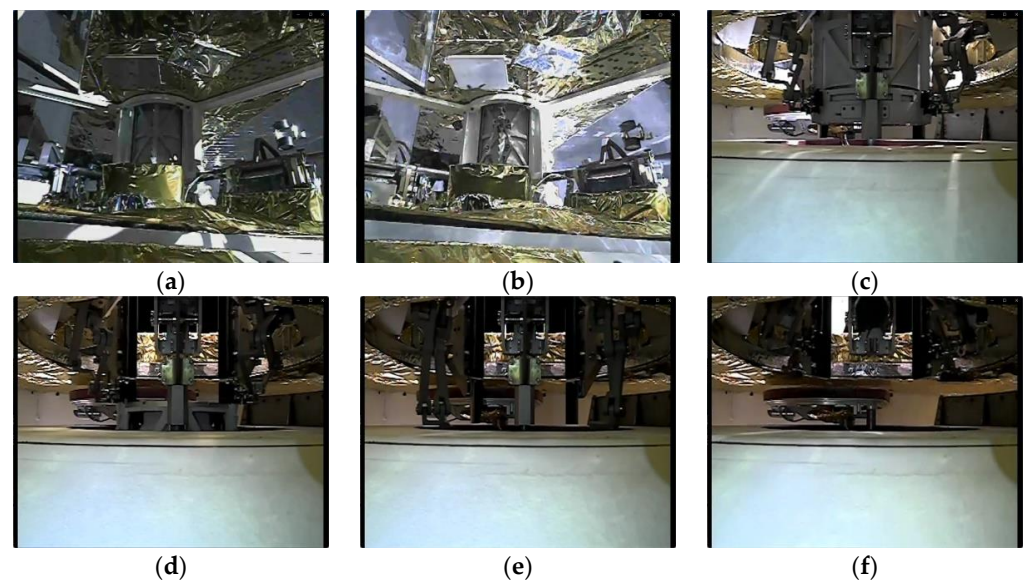


Figure 19. In-orbit flight validation of transfer mechanism. (a) Docking complete. (b) The transfer mechanism captures the container. (c) Container passes through the orbiter. (d) Container enters the re-entry vehicle. (e) Container transfer in place. (f) Retraction of the mechanism and the guide rail.

5. Conclusions

Aiming at the automatic sample transfer mission of lunar sample return in lunar orbit, a pawl composite linkage transfer mechanism is designed, which can realize the sample container in-orbit transfer. The design focuses on the whole process resistance and the sensitive factors of resistance during the transfer process. The sample transfer process was verified using a ground test system, indicating that the design could well adapt to the requirements of the sample transfer mission. The designed transfer mechanism successfully completed the flight mission in a good working state, which further verifies the correctness and effectiveness of the design. Through the design of the transfer path and the transfer mechanism, the difficulties of lightweight, long stroke, and highly reliable multi-constraint design have been solved, which provides a good reference for the subsequent design of various types of in-orbit sample transfer.

Author Contributions: Conceptualization, W.W.; data curation, Y.C. (Yanyan Cao); funding acquisition, C.Z.; investigation, Y.C. (Yuxin Cui) and S.W.; methodology, W.W., C.Q., Y.Z. and C.Z.; project administration, Y.Z. and C.Z.; resources, Y.C. (Yuxin Cui); software, W.W.; supervision, C.Q. and S.W.; validation, W.W. and C.Q.; visualization, Y.C. (Yanyan Cao); writing—original draft, W.W., Y.C. (Yuxin Cui), C.Q., Y.C. (Yanyan Cao), Y.Z., C.Z. and S.W.; writing—review and editing, W.W. and C.Q. All authors have read and agreed to the published version of the manuscript.

Funding: This research was funded by the National Natural Science Foundation of China, grant number 51975351.

Data Availability Statement: The data presented in this study are available on request from the corresponding author. The data are not publicly available due to privacy restrictions.

Conflicts of Interest: C.Z. are employed by the China Aerospace Science and Technology Group Co., Ltd. The remaining authors declare that the research was conducted in the absence of any commercial or financial relationships that could be construed as a potential conflict of interest.

References

1. Mallapaty, S. China set to retrieve first Moon rocks in 40 years. *Nature* **2020**, *587*, 185–186. [[CrossRef](#)]
2. Yang, M.; Zhang, G.; Zhang, W.; Peng, J.; Ruan, J.; Wang, Y.; Zhang, H.; Hong, X.; Zhang, Y.; Zha, X.; et al. Technical design and implementation of Chang'e-5 robotic sample return mission on lunar surface. *Sci. Sin. Technol.* **2021**, *51*, 738–752. (In Chinese) [[CrossRef](#)]
3. Yang, W.; Lin, Y. New lunar samples returned by Chang'E-5: Opportunities for new discoveries and international collaboration. *Innovation* **2021**, *2*, 100070. [[CrossRef](#)]
4. Siddiqi, A.A.; Launius, R. *Deep Space Chronicle: A Chronology of Deep Space and Planetary Probes 1958–2000*. Military Bookshop: Washington, DC, USA, 2002.
5. Robinson, M.S.; Plescia, J.B.; Jolliff, B.L.; Lawrence, S.J. Soviet lunar sample return missions: Landing site identification and geologic context. *Planet. Space Sci.* **2012**, *69*, 76–88. [[CrossRef](#)]
6. Scherer, L.R. The Apollo Missions. *Highlights Astron.* **2016**, *2*, 125–141. [[CrossRef](#)]
7. Shaw, M.; Humbert, M.; Brooks, G.; Rhamdhani, A.; Duffy, A.; Pownceby, M. Mineral processing and metal extraction on the lunar surface-challenges and opportunities. *Miner. Process. Extr. Metall. Rev.* **2022**, *43*, 865–891. [[CrossRef](#)]
8. Li, C.; Hu, H.; Yang, M.; Pei, Z.; Zhou, Q.; Ren, X.; Liu, B.; Liu, D.; Zeng, X.; Zhang, G. Characteristics of the lunar samples returned by the Chang'E-5 mission. *Natl. Sci. Rev.* **2022**, *9*, nwab188. [[CrossRef](#)] [[PubMed](#)]
9. Carlson, R.W. Robotic sample return reveals lunar secrets. *Nature* **2021**, *600*, 39–40. [[CrossRef](#)]
10. Ji, M.; Wang, C.; Sun, L. A structure used for the sealing and locking of lunar samples. In Proceedings of the 2018 International Conference on Service Robotics Technologies, Chengdu, China, 16–19 March 2018; pp. 38–41.
11. Wang, W.; Zhang, C.; Qi, C.; Fu, L.; Wang, S. Stiffness design of active capture claw-type docking mechanism for lunar sample return. *Aerospace* **2023**, *10*, 794. [[CrossRef](#)]
12. Qi, C.; Li, D.; Hu, Y.; Zheng, Y.; Wang, W.; Shou, X.; Gao, F. Learning-based distortion compensation for a hybrid simulator of space docking. *IEEE Robot. Autom. Lett.* **2023**, *8*, 3446–3453. [[CrossRef](#)]
13. Cao, Y.; Fu, L.; Wang, W.; Liu, Z.; Liu, Z. End precision optimization method and its on-orbit application of sample transfer mechanism. *Aerosp. Shanghai* **2022**, *39*, 61–66.
14. Stieberl, M.E. Robotic systems for the international space station. In Proceedings of the 1997 IEEE International Conference on Robotics and Automation, Albuquerque, NM, USA, 20–25 April 1997; pp. 3068–3073.
15. Laryssa, P.; Lindsay, E.; Layi, O.; Marius, O.; Nara, K.; Aris, L.; Ed, T. International space station robotics: A comparative study of ERA, JEMRMS and MSS. In Proceedings of the 7th ESA Workshop on Advanced Space Technologies for Robotics and Automation, Noordwijk, The Netherlands, 19–21 November 2002; pp. 1–8.
16. Oda, M.; Inaba, N. Results of NASDA's ETS-VII robot mission and its applications. In *Robotics Research*; Hollerbach, J.M., Koditschek, D.E., Eds.; Springer: London, UK, 2000. [[CrossRef](#)]
17. Moghaddam, B.M.; Chhabra, R. On the guidance, navigation and control of in-orbit space robotic missions: A survey and prospective vision. *Acta Astronaut.* **2021**, *184*, 70–100. [[CrossRef](#)]
18. Xue, Z.; Liu, J.; Wu, C.; Tong, Y. Review of in-space assembly technologies. *Chin. J. Aeronaut.* **2021**, *34*, 21–47. [[CrossRef](#)]
19. Qi, X.; Huang, H.; Miao, Z.; Li, B.; Deng, Z. Design and mobility analysis of large deployable mechanisms based on plane-symmetric Bricard linkage. *J. Mech. Des.* **2017**, *139*, 022302. [[CrossRef](#)]
20. Gosselin, C.; Schreiber, L.-T. Redundancy in parallel mechanisms: A review. *Appl. Mech. Rev.* **2018**, *70*, 010802. [[CrossRef](#)]

Disclaimer/Publisher's Note: The statements, opinions and data contained in all publications are solely those of the individual author(s) and contributor(s) and not of MDPI and/or the editor(s). MDPI and/or the editor(s) disclaim responsibility for any injury to people or property resulting from any ideas, methods, instructions or products referred to in the content.